

Global nonlinear gyrokinetic simulations of electromagnetic turbulence in tokamaks and stellarators

A. Bottino¹, M. Borchardt², T.B. Fehér², R. Hatzky¹, K. Kauffmann², R. Kleiber², A. Könies², A. Mishchenko², A. G. Peeters³, E. Poli¹, B. Scott²

¹ Max-Planck-Institut für Plasmaphysik, EURATOM Association, 85748 Garching, Germany

² Max-Planck-Institut für Plasmaphysik, EURATOM Association, 17491 Greifswald, Germany

³ University of Bayreuth, 95440 Bayreuth, Germany

e-mail: alberto.bottino@ipp.mpg.de

Abstract In this paper we discuss global linear and nonlinear gyrokinetic results concerning effects of finite beta and collisions in tokamak and stellarator turbulence, using particle in cell (PIC) codes. Our approach is based on an adjustable control variate method which drastically reduces the computational resources needed to correctly describe the evolution of the non-adiabatic currents and limits the growth of the discretization error. Global electromagnetic and collisional PIC simulations of realistic plasmas can finally be achieved.

1. Introduction.

The theoretical understanding of mesoscale and microscale turbulence is required for developing a predictive capability of heat, particle and momentum transport in tokamaks and stellarators. Many global linear and nonlinear particle in cell (PIC) codes are routinely used for solving the gyrokinetic equations in the limit of the electrostatic approximation. However, the electrostatic approximation is expected to break down in the core of high β_e ($\beta_e \equiv \mu_0 n_e T_e / B^2$) plasmas or in any region where pressure gradients are large. For a finite value of β_e , magnetic fluctuations modify the evolution of the electrostatic instabilities and eventually introduce new electromagnetic modes [1]. Therefore, a complete electromagnetic treatment of plasma instabilities is desirable and must be included in models and codes. Most of the existing gyrokinetic PIC codes are based on the δf method [2–4]. In the δf method the distribution function f of each plasma species is split into a time independent background distribution function f_0 and a time dependent perturbation δf , $f = f_0 + \delta f$. In the δf method, the perturbed part only (δf) is discretized using numerical particles. As long as the perturbation δf remains small as compared to f_0 , the δf method reduces the statistical noise. The δf method can be interpreted as a “control variate” algorithm [5,6], a variance reduction technique widely used for Monte Carlo methods. Electromagnetic simulations using a conventional δf method are much more demanding in respect of numerical resources than electrostatic simulations. The parallel electron dynamics imposes a strong constraint on the size of the time step. In addition to this, electromagnetic simulations require a much larger number of numerical particles in order to correctly describe the evolution of the non-adiabatic part of the electron distribution function. Indeed, the physically relevant non-adiabatic part of the electron distribution function is overwhelmed by the adiabatic response to the magnetic potential A_{\parallel} leading to a severe accuracy problem, known in the literature as the “cancellation problem” (see [6] and references therein). Two main methods have been proposed to overcome those difficulties: the so called “split-weight” scheme, originally proposed in [7], and the use of an appropriate adjustable control variate method in the conventional δf scheme [6]. The adjustable control variate method has been applied in linear electromagnetic tokamak simulations using the code GYGLES [8]. The same method has been successfully extended to nonlinear simulations using NEMORB[9], a new electromagnetic, multispecies version of the code ORB5 [10], as well as to the full 3D global code EUTERPE[11]. In this paper we present an overview of the recent

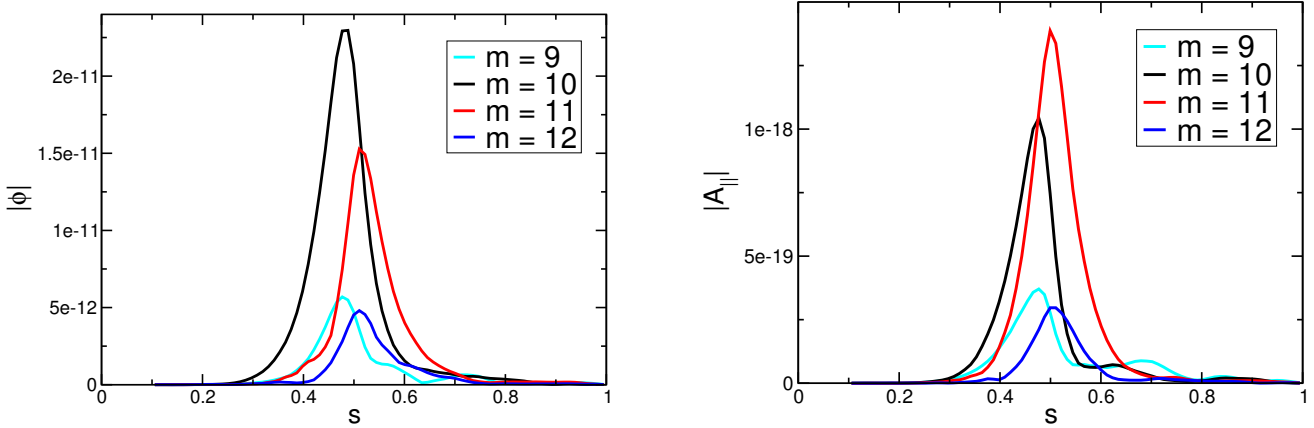


Figure 1: radial structure of the electrostatic potential (left) and parallel magnetic potential (right) for a TAE mode, GYGLES simulation [12].

results obtained by the three global codes GYGLES, NEMORB and EUTERPE, all based on improved control variate schemes.

The organization of the paper is as follows. In Sec.II the gyrokinetic model used in the codes is presented. Section III is dedicated to the discussion of linear simulations of shear Alfvén modes, focusing in particular on fast-particle effects. Nonlinear simulations of finite- β_e microturbulence are presented in section IV. Finally, the influence of collisions on ion temperature gradient (ITG) modes in stellarator geometry is discussed in section V.

2. The gyrokinetic model

Our gyrokinetic model is based on the gyrokinetic Vlasov-Maxwell system of equations of Hahm and Brizard [13–16]. The latter consists of a set of self-consistent and energy conserving nonlinear gyrokinetic equations for particles and fields.

The particle Lagrangian is

$$L \equiv (e\mathbf{A} + p_z \mathbf{b}) \cdot \dot{\mathbf{R}} + \frac{m^2}{e} \mu \dot{\theta} - H \quad (1)$$

where $(\mathbf{R}, p_z, \mu, \theta)$ are the particle coordinates, \mathbf{b} is the unit vector for \mathbf{B} , m and e are the species mass and charge. Here, $\mu \equiv v_\perp^2 / 2B$ is magnetic moment per unit mass and p_z is the canonical parallel momentum coordinate, defined by:

$$mU \equiv p_z - eJ_0 A_\parallel, \quad U = \frac{\partial H}{\partial p_z} \quad (2)$$

U is the parallel velocity of the particle and J_0 is the gyroaverage operator.

The Hamiltonian contains only terms up to the first order in the potential fields, Φ and A_\parallel :

$$H = m \frac{U^2}{2} + m\mu B + eJ_0 \Phi + O(\Phi^2) \simeq \frac{1}{2m} [p_z^2 - 2ep_z J_0 A_\parallel] + m\mu B + eJ_0 \Phi. \quad (3)$$

The equations of motion are given by the Euler-Lagrange equations:

$$\dot{\mathbf{R}} = \frac{\partial H}{\partial p_z} \frac{\mathbf{B}^*}{B_\parallel} - \frac{1}{eB B_\parallel^*} \mathbf{F} \cdot \nabla H \quad (4)$$

$$\dot{p}_z = -\frac{\mathbf{B}^*}{B_\parallel} \cdot \nabla H \quad (5)$$

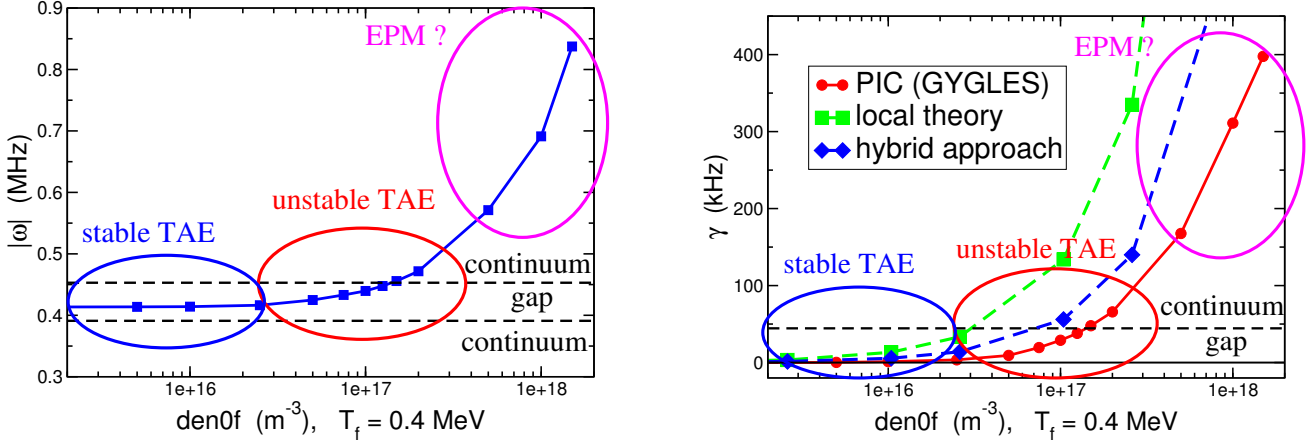


Figure 2: real frequency (left) and the growth rate (right) of the TAE mode destabilized by fast particles as a function of fast particle density, GYGLES simulation [12]. The fast-particle destabilization of the TAE mode and modification of the TAE into the EPM instability has been observed in the simulations.

we have used a tensor notation for the magnetic field, summarized by:

$$\mathbf{F} = \nabla \mathbf{A} - (\nabla \mathbf{A})^T \quad \mathbf{F} = \varepsilon \cdot \mathbf{B} \quad \nabla \times \mathbf{b} = -\nabla \cdot \frac{\mathbf{F}}{B} \quad \mathbf{b} \times = -\frac{\mathbf{F}}{B}. \quad (6)$$

Replacing the Hamiltonian of Eq. (3) in the Euler-Lagrange equations (4) and defining a generalized potential Ψ , the equations of motion become:

$$\Psi \equiv \Phi - \frac{p_z}{m} A_{\parallel} \quad (7)$$

$$\dot{\mathbf{R}} = \left(\frac{p_z}{m} - \frac{e}{m} J_0 A_{\parallel} \right) \frac{\mathbf{B}^*}{B_{\parallel}^*} + \frac{1}{B_{\parallel}^*} \mathbf{b} \times \left[\mu \frac{m}{e} \nabla B + \nabla J_0 \Psi \right] \quad (8)$$

$$\dot{p}_z = -\frac{m \mathbf{B}^*}{B_{\parallel}^*} \cdot \left[\mu \nabla B + \frac{e}{m} \nabla J_0 \Psi \right] \quad (9)$$

where $\mathbf{B}^* = \nabla \times \mathbf{A}^*$ and $\mathbf{A}^* \equiv \mathbf{A} + (p_z/e) \mathbf{b}$.

The gyrokinetic Vlasov equation is:

$$\frac{dF}{dt} = \frac{\partial F}{\partial \mathbf{R}} \cdot \dot{\mathbf{R}} + \frac{\partial F}{\partial p_z} \dot{p}_z = C(F) + S \quad (10)$$

where $F(\mathbf{R}, p_z, \mu)$ is the distribution function of the gyrocenters, $C(F)$ is a collision operator and S is a source term. The time evolution of the perturbed electrostatic and magnetic potentials is described by the linearized gyrokinetic Poisson equation (in the long wavelength approximation) and by the parallel Ampère's law, respectively:

$$-\nabla_{\perp} \left(\sum_{\text{species}} \frac{m n_0}{e B^2} \right) \nabla_{\perp} \Phi = \sum_{\text{species}} \delta n \quad (11)$$

$$\left(\sum_{\text{species}} \frac{\mu_0 n_0 e^2}{m} A_{\parallel} \right) - \nabla_{\perp}^2 A_{\parallel} = \mu_0 \sum_{\text{species}} \delta j_{\parallel} \quad (12)$$

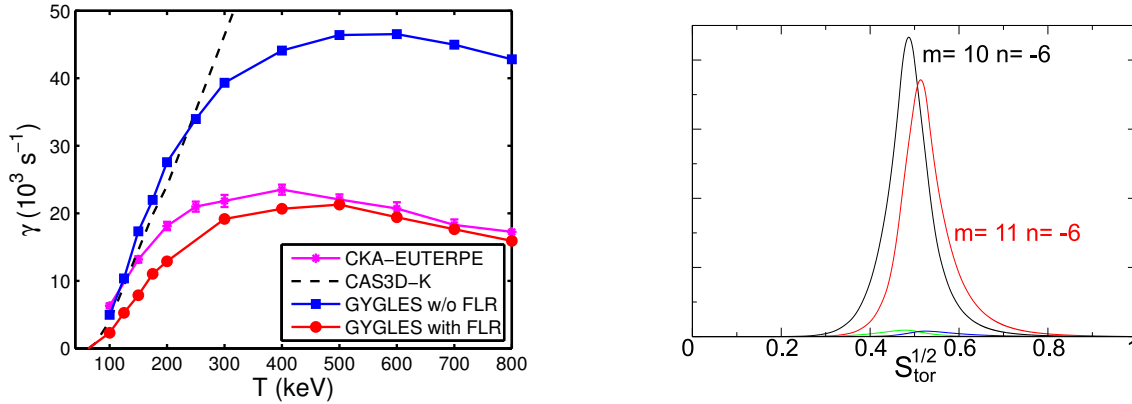


Figure 3. (a) growth rate of a TAE mode as a function of fast particle temperature, for different codes. Good agreement is found between CKA-EUTERPE and GYGLES. (b) radial mode structure, $|\phi(s)|$ [arbitrary units], for $T = 400$ KeV, calculated by CKA-EUTERPE; s_{tor} is the normalized toroidal flux.

where $\delta n = \int dW \delta f \delta(\mathbf{R} + \boldsymbol{\rho} - \mathbf{x})$ is the perturbed gyrocenter density, $\delta j_{\parallel} = e \int dW (p_z/m) \delta f \delta(\mathbf{R} + \boldsymbol{\rho} - \mathbf{x})$, $dW = 2\pi B_{\parallel}^* m^{-1} d\mathbf{R} dp_z d\mu$ and $\boldsymbol{\rho}$ is the gyroradius. For $C(F) = 0$ and $S = 0$, this set of gyrokinetic equations is energy and momentum conserving. An elegant proof is given in Ref. [17].

3. Linear global simulations of Alfvén modes in tokamak

The GYGLES [18] code has been successfully used to perform global simulations of shear Alfvén modes in tokamak and pinch geometry. Figure 1 shows an example of toroidal Alfvén eigenmode (TAE) for a large aspect ratio tokamak. The mode is radially located in the vicinity of the position of the gap in the shear Alfvén spectrum. The mode shows the typical radial structure of a TAE. Moreover, the dominant frequency is in agreement with the frequency of the corresponding ideal MHD mode. A detailed description of this simulation and the corresponding numerical and physical parameters, can be found in Refs. [12,18].

When a fast particle population is present in the simulation, the TAE mode is destabilized by fast particles above a certain threshold density. This effect is illustrated in Fig. 2, where the real part of the frequency and the growth rate of the most unstable modes are plotted as a function of the fast particle density. An increase in the fast particle density leads to a further destabilization of the TAE. When the fast particle density is large enough, the most unstable mode becomes an energetic particle continuum mode (EPM). Note that an increase of the fast ion temperature leads to similar results. Details can be found in Ref. [12].

In the framework of a perturbative approach to the destabilization of Alfvén modes by fast particles a module has been developed to couple EUTERPE to an ideal three-dimensional MHD code like the CKA code. The energy transfer between fast particles and the ideal MHD mode is then calculated to yield the growth rate. First benchmarks show good agreement with other codes. Figure 3 shows an example of a direct comparison between GYGLES and the CKA-EUTERPE hybrid code. In Fig. 3 (a), the growth rate of the most unstable mode has been calculated for different values of the fast particle temperature. The two codes are in good agreement even for large values of the fast particle temperature. This illustrates the importance

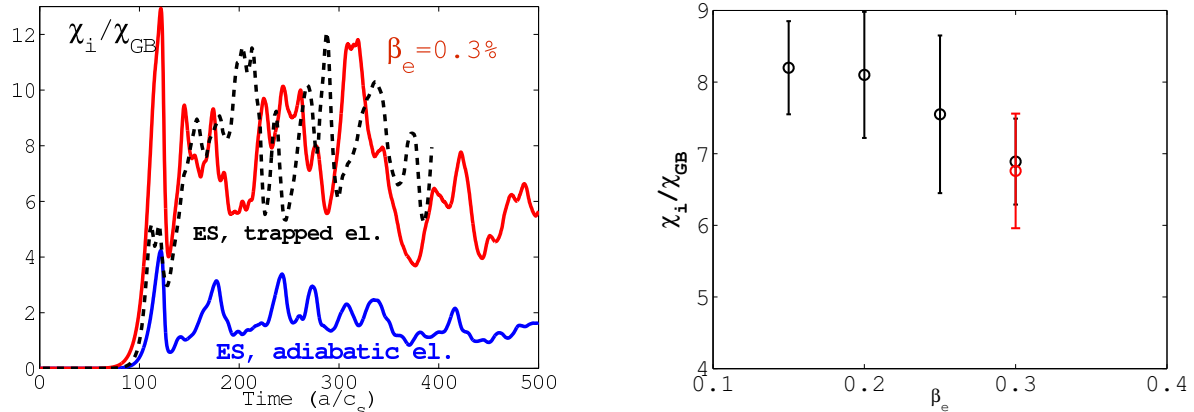


Figure 4. (a) time evolution of the ion thermal diffusivity for an electromagnetic $\beta_e = 0.3\%$ simulation (red), and electrostatic simulation with (black, dashed) and without (blue) trapped electrons, copyright ©2010 IEEE. (b) ion thermal diffusivity as a function of β_e , moving averaged in time. The red point corresponds to a simulation with different initial conditions.

of retaining finite Larmor radius (FLR) effects in the simulations. For comparison, results of the hybrid MHD-drift kinetic code CAS3D-K [19] are shown, where finite orbit width and FLR effects had been neglected. Figure 3 (b) gives an example of a radial mode structure calculated by CKA, in good agreement with the GYGLES code.

4. Nonlinear finite β_e simulations of microturbulence in tokamaks

The nonlinear PIC code ORB5 solves the set of nonlinear gyrokinetic equations in the whole plasma core down to the magnetic axis, using MHD equilibria. The dissipation necessary to assure entropy saturation is provided by a residual zonal flow conserving noise-control algorithm [20,21]. The code ORB5 has been proved to scale up to 32k cores on a BlueGene/P architecture. The electromagnetic version of ORB5, NEMORB, has been tested and benchmarked against the linear electromagnetic code GYGLES [9]. The nonlinear simulations described in this Section, are based on parameters and profiles of the Cyclone base case [22]. The mass ratio is $m_i/m_e = 1000$ and the value of the central density has been adjusted to have $\beta_e = 0.3\%$. Figure 4 (a) compares the time evolution of ion thermal diffusivity of a $\beta_e = 0.3\%$ electromagnetic simulation (red) with the the original electrostatic, adiabatic electrons simulation of Ref. [22] (blue) and an electrostatic simulation including kinetic trapped electrons (black). The ion thermal diffusivity for the electrostatic simulation including trapped electrons is comparable with the electromagnetic case. The EM simulation (red) was performed using 512 million numerical particles per species and with a time step 20 times smaller than the electrostatic case ($\Delta t = 1 \Omega_i$ where Ω_i is the ion cyclotron frequency). Figure 4 (b) presents a scan in β_e for the ion diffusivity, for the same parameters of Fig. 4 (a). β_e has been varied by rescaling the value of the density on the axis. A heating source is applied, in order to prevent profile relaxation. The ion diffusivities have been averaged in radius, over the range $s = [0.6, 0.8]$ (s is the square root of normalized poloidal flux) and in time, using a moving time window during the stationary phase of the simulations. The two points at $\beta_e = 0.3\%$ correspond to different initial conditions: white noise (black) and single mode initialization (red). The stabilizing effect of finite β_e on ITGs, already documented in many linear simulation, is recovered in global nonlinear simulations.

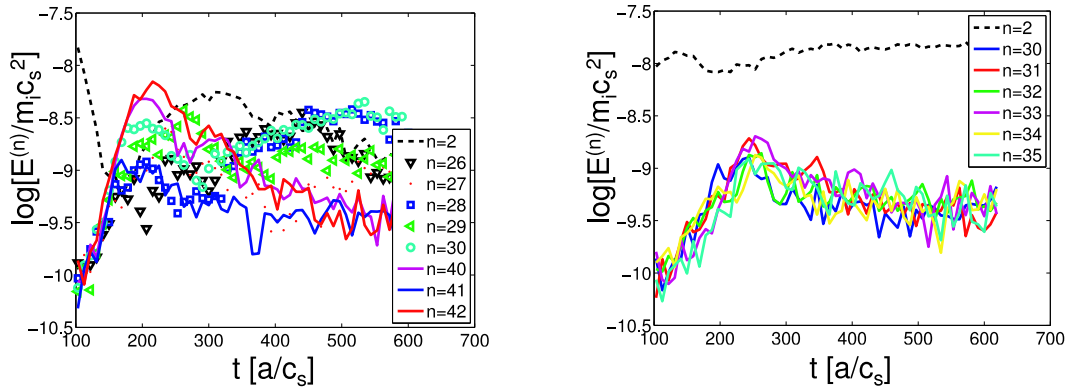


Figure 5: time evolution of the field energy at a radial position far from the island (left) and at the island separatrix (right) [23].

Magnetic islands, supposed to evolve on a much longer time scale than the turbulence, have been introduced in ORB5 through a time-independent parallel vector potential A_{\parallel} of assigned helicity. Simulations of electrostatic turbulence including a magnetic island have demonstrated the nonlinear excitation of (otherwise linearly stable) long-wavelength modes, corresponding to the mode numbers of the rational surface under consideration. The sheared flows associated to these large-scale modes “rip apart” the eddies in analogy to what is known from zonal-flows dynamics. Fig. 5 reports the time evolution of the local turbulence spectrum at two different radial locations, the first at a given distance from the island, the second at the island separatrix. In the first case, it can be seen that the $n = 2$ component of the electrostatic potential, that decays during the first phase of the ORB5 simulation (in which the profiles adjust to the perturbed equilibrium[23]), raises again due to the nonlinear pumping mentioned above. However, the energy of the long-scale mode is smaller than that of turbulence during most of the simulation time and the turbulent eddies efficiently transport heat across the flux surfaces. On the contrary, at the island separatrix, the $n = 2$ mode largely dominates. The result observed in several simulations is a reduction of the heat flux at the separatrix, except for the X-point region, where larger structures can develop. From the simulations performed so far with ORB5 and GKW[24,25], however, no firm conclusion can be drawn on whether nonlinearly generated sheared flows arising in the presence of small magnetic islands can contribute to the improvement of the confinement in the vicinity of rational surfaces, which has been reported in experiments[26].

5. Influence of collisions on ITG modes in stellarators

The full 3D global gyrokinetic code EUTERPE uses stellarator equilibria calculated with VMEC. The mapping from VMEC to the internally used PEST coordinates is done by a newly developed tool allowing the use of smoothed splines to make the equilibrium more consistent near the magnetic axis. The physical model of EUTERPE includes three kinetic species, nonlinear terms and electromagnetic perturbations. A pitch angle collision operator can also be included to allow e.g. neoclassical transport calculations or the simulation of collisional effects on TEM and ITGs. Benchmarks of the electromagnetic version using analytically given equilibria for destabilized GAE and TAE show good agreement with the GYGLES code for different β_e . The code EUTERPE has been used to study the effect of collisions on 3D configurations.

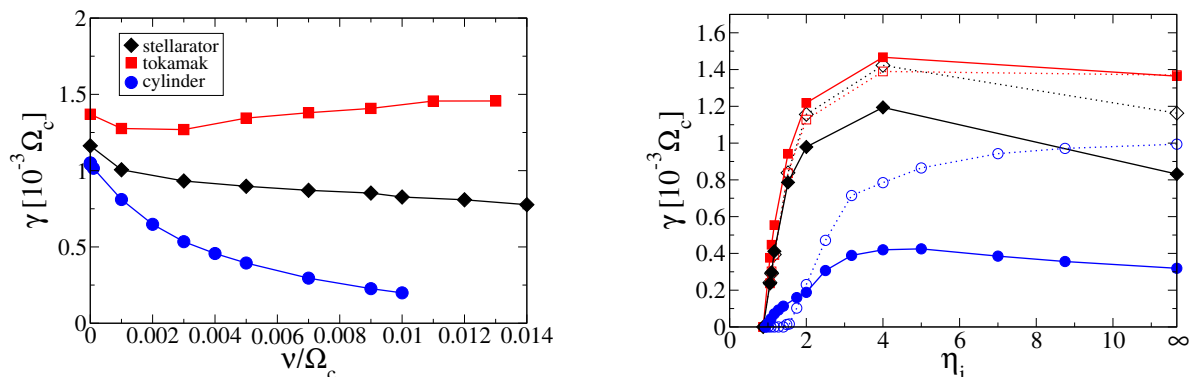


Figure 6. Left: Growth rate dependence on collisionality for different geometries ($L_T/a = 0.0, L_T/a = 3.5$). Right: Growth rate dependence on η_i (for fixed $L_T/a = 3.5$) for a cylinder (blue), a tokamak (red) and a stellarator (black) configuration. Dotted lines and open symbols indicate the collisionless case. Solid lines and filled symbols indicate the collisional case ($\nu = 0.01 \Omega_i$).

The stellarator results presented in Fig. 6 correspond to a LHD configuration with $R = 3.75$ m and $\beta_e = 1.5\%$. This configuration has been compared with an equivalent tokamak of aspect ratio $A = 5$ and minor radius $a = 0.8$ m, and a cylinder of $A = 5$ and $a = 0.8$ m, but having a flat iota profile. Figure 6, left, shows the dependency of the growth rate on the collisionality ν . A weakly stabilizing effect of the collisionality for the dominant ITG mode is present in stellarator configuration. Figure 6 (right) illustrates the effect of varying $\eta_i \equiv L_n/L_T$, where L_T and L_n are the equilibrium temperature and density gradient scale lengths, respectively. For stellarators, collisions provide a stronger stabilization to the ITG mode for larger values of η_i . The behavior is different in tokamak configurations, where, in general, the ITG is always weakly affected by collisions. The poloidal cross section of the electrostatic potential at different toroidal positions, for the collisional LHD simulation, is shown in Fig. 7.

6. Conclusions

Gyrokinetic global PIC simulations have made dramatic progress in the last years. In particular, the problem of the accumulation of the numerical noise has been cured by introducing dissipation in the Lagrange discretization. Moreover, the use of adjustable control variate methods, drastically reduces the numerical resources required for electromagnetic and collisional simulations. In this paper, we have presented a brief overview of results obtained by applying both noise reduction techniques and control variate methods. The results suggest that global nonlinear electromagnetic simulations in realistic tokamak and stellarator configurations are finally achievable.

Acknowledgments

Nonlinear simulations were performed on the CRAY XT4/XT5 Louhi at CSC, Finland, in the frame of the DEISA-Extreme Computing Initiative and on the HPC-FF JUROPA server at the Jülich Rechenzentrum under EFDA. EUTERPE simulations have been performed on the IBM Power6 (SP6) at CINECA, Italy, in the frame of the DEISA-Extreme Computing Initiative. We thank P. Helander, B.F. McMillan, L. Villard and S. Jolliet for helpful discussions.

References

- [1] ZONCA, F. et al., Physics of Plasmas **6** (1999) 1917.

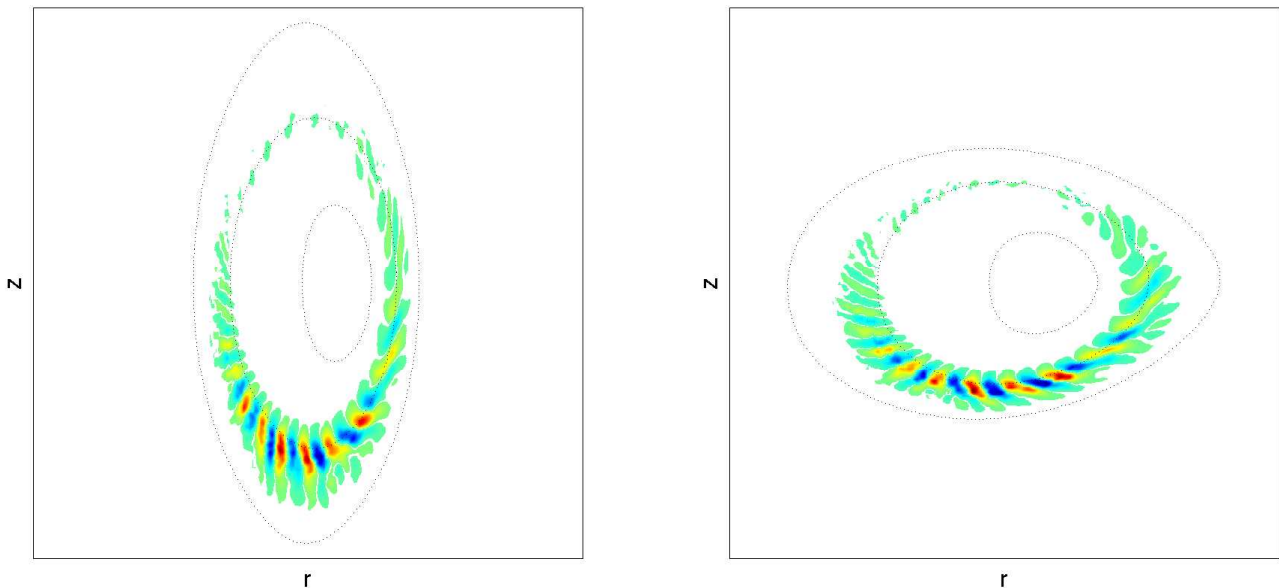


Figure 7: real part of the electrostatic potential for the collisional ($\nu = 0.01 \Omega_i$) ITG mode in LHD. Left: Cross section at the beginning of a period ($\varphi = 0$). Right: cross section at the middle of a period ($\varphi = \frac{1}{2} \frac{2\pi}{10}$).

- [2] LEE, W. W., Physics of Fluids **26** (1983) 556.
- [3] PARKER, S. E. et al., Physics of Fluids B **5** (1993) 77.
- [4] DIMITS, A. M. et al., Journal of Computational Physics **107** (1993) 309.
- [5] AYDEMIR, A. Y., Physics of Plasmas **1** (1994) 5480.
- [6] HATZKY, R. et al., Journal of Computational Physics **189** (2007) 463.
- [7] CHEN, Y. et al., Journal of Computational Physics **189** (2003) 463.
- [8] MISHCHENKO, A. et al., Physics of Plasmas **11** (2004) 5480.
- [9] BOTTINO, A. et al., IEEE Transactions on Plasma Science **38** (2010) 2129.
- [10] JOLLIET, S. et al., Computer Physics Communications **177** (2007) 409.
- [11] KORNILOV, V. et al., Physics of Plasmas **11** (2004) 3196.
- [12] MISHCHENKO, A. et al., Physics of Plasmas **16** (2009) 082105.
- [13] HAHM, T. S. et al., Physics of Fluids **31** (1988) 1940.
- [14] HAHM, T. S., Physics of Fluids **31** (1988) 2670.
- [15] BRIZARD, A., Journal of Plasma Physics **41** (1989) 541.
- [16] SUGAMA, H., Physics of Plasmas **7** (2000) 466.
- [17] SCOTT, B. et al., Phys. Plasmas **17** (2010) in press, arXiv:1008.1244.
- [18] MISHCHENKO, A. et al., Physics of Plasmas **15** (2008) 112106.
- [19] KÖNIES, A., Physics of Plasmas **7** (2000) 1139.
- [20] MCMILLAN, B. F. et al., Physics of Plasmas **16** (2009) 022310.
- [21] JOLLIET, S. et al., Physics of Plasmas **16** (2009) 052307.
- [22] FALCHETTO, G. L. et al., Plasma Physics and Controlled Fusion **50** (2008) 124015.
- [23] POLI, E. et al., Nuclear Fusion **49** (2009) 075010.
- [24] HORNSBY, W. A. et al., Physics of Plasmas **17** (2010) 092301.
- [25] POLI, E. et al., Plasma Physics and Controlled Fusion **52** (2010) accepted for publication.
- [26] JOFFRIN, E. et al., Nuclear Fusion **43** (2003) 1167.